Acoustic streaming in a microfluidic channel with a reflector: Case of a standing wave generated by two counterpropagating leaky surface waves

Alexander A. Doinikov, Pierre Thibault, and Philippe Marmottant
LIPhy, UMR 5588, CNRS/Université Grenoble-Alpes, Grenoble F-38401, France
(Received 4 April 2017; published 5 July 2017)

A theory is developed for the modeling of acoustic streaming in a microfluidic channel confined between an elastic solid wall and a rigid reflector. A situation is studied where the acoustic streaming is produced by two leaky surface waves that propagate towards each other in the solid wall and thus form a combined standing wave in the fluid. Full analytical solutions are found for both the linear acoustic field and the field of the acoustic streaming. A dispersion equation is derived that allows one to calculate the wave speed in the system under study. The obtained solutions are used to consider particular numerical examples and to reveal the structure of the acoustic streaming. It is shown that two systems of vortices are established along the boundaries of the microfluidic channel.

DOI: 10.1103/PhysRevE.96.013101

I. INTRODUCTION

The phenomenon of acoustic streaming is widely applied in microfluidic devices for the implementation of such processes as micromixing of fluids and contactless manipulation of microparticles suspended in a fluid [1–6]. There is a long-standing interest in acoustic streaming that arises in the course of wave propagation between two boundaries. Rayleigh [7] was the first to theoretically study this problem for the case of a plane standing wave propagating between two plane rigid walls. The vortex pattern outside the viscous boundary layer predicted by his theory is known as Rayleigh streaming. Later, this problem also was considered by Westervelt [8] and Nyborg [9,10]. The solutions obtained by Rayleigh, Westervelt, and Nyborg are valid for channels with a relatively large distance between the walls in which the boundary layer thickness is negligible in comparison with the interwall distance. Hamilton *et al.* [11] derived an analytical solution for acoustic streaming generated by a standing wave between two rigid walls with an arbitrary interwall distance. Their theory shows that, as the distance between the walls is reduced, the streaming vortices inside the boundary layer increase in size relative to the Rayleigh streaming vortices outside the boundary layer and, for interwall distances less than about ten times the boundary layer thickness, the Rayleigh vortices disappear and only the inner vortices exist. Recently, Doinikov *et al.* [12] have generalized the approach of Hamilton *et al.* [11] to the case of two orthogonal standing waves. They showed that the acoustic streaming gives rise to rotational fluid motion in planes parallel to the walls. As a result, fluid particles, when moving up and down between the walls, are rotating about axes perpendicular to the walls.

However, the generation of acoustic streaming in microfluidic devices is realized under conditions different from those considered in the above-mentioned papers. To induce acoustic waves in a microfluidic channel, leaky surface waves are used, which are excited in a solid substrate and emit into the fluid layer through the vibrations of the solid-fluid interface [13]. The speed of the leaky surface waves and hence that of acoustic waves induced in the fluid are different from the normal speed of sound in the fluid and are determined by a dispersion equation. The dispersion equation for a half-infinite inviscid fluid layer can be found, for example, in the book by Viktorov [14] and that for a finite viscous layer with a free boundary was derived by Qi [15]. A dispersion equation for a microfluidic channel with a reflector is derived here. Vanneste and Bühler [16] obtained linear analytical solutions and then performed a numerical modeling of acoustic streaming for the case of one leaky surface wave and a fluid layer with a free boundary.

In the present paper, we consider a fluid layer confined between an elastic solid wall and a rigid reflector. We derive solutions for leaky surface waves in the solid wall, a dispersion equation for the speed of these waves, and linear solutions for acoustic waves in the fluid. We then solve the equations of acoustic streaming assuming that this latter is produced by a standing wave that is generated by two counterpropagating leaky surface waves as is the case in microfluidic devices. All the solutions are analytical and valid for the entire section of the fluid channel without splitting it into the bulk part and viscous boundary layers. No restrictions are imposed on the value of the fluid viscosity.

II. THEORY

A. Problem formulation

Let us assume that a fluid layer is confined between an elastic solid wall and a rigid reflector (see Fig. 1). We will first consider a plane harmonic surface wave that is excited in the solid wall and propagates in the positive direction of the x axis, the z axis being directed perpendicular to the fluid-solid interface into the depth of the solid wall. The results obtained for this wave will then be applied to two counterpropagating waves in order to get a combined standing wave. We assume that the solid wall occupies the half-space $z > 0$ and the fluid layer occupies the space $0 > z > -h$.

B. Linear solutions

1. Waves in the fluid

If the fluid is treated as compressible and viscous, the linearized equations of the fluid motion are

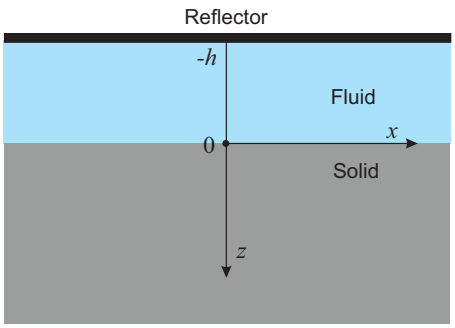

FIG. 1. A fluid layer of height h is located between an elastic solid wall and a rigid reflector. A surface acoustic wave is excited in the solid wall and propagates along the x axis.

given by [17]

$$\rho_f \frac{\partial \boldsymbol{v}}{\partial t} = -\nabla p + \eta\, \Delta \boldsymbol{v} + (\xi + \eta/3)\nabla(\nabla \cdot \boldsymbol{v}), \quad (1)$$

$$\frac{\partial \rho}{\partial t} + \rho_f \nabla \cdot \boldsymbol{v} = 0, \quad (2)$$

$$p = c_f^2 \rho, \quad (3)$$

where Eqs. (1)–(3) are the Navier-Stokes equation, the continuity equation, and the equation of state, respectively, ρ_f is the fluid density at rest, $\boldsymbol{v}$ is the fluid velocity, p is the perturbed fluid pressure, η is the shear viscosity, ξ is the bulk viscosity, ρ is the perturbed fluid density, and c_f is the speed of sound.

Let us set the time dependence as $\exp(-i\omega t)$ and represent $\boldsymbol{v}$ as

$$\boldsymbol{v} = \nabla \varphi_f + \nabla \times \boldsymbol{\psi}_f, \quad (4)$$

where φ_f and $\boldsymbol{\psi}_f$ are the scalar and the vector potentials. Substituting Eq. (4) into Eqs. (1)–(3) after some manipulations, one obtains

$$\Delta \varphi_f + k_f^2 \varphi_f = 0, \quad (5)$$

$$\Delta \boldsymbol{\psi}_f + k_v^2 \boldsymbol{\psi}_f = 0, \quad (6)$$

$$p = \frac{i}{\omega} \rho_f c_f^2 k_f^2 \varphi_f, \quad (7)$$

where

$$k_f = \frac{\omega}{c_f}\left[1 - \frac{i\omega}{\rho_f c_f^2}\left(\xi + \frac{4}{3}\eta\right)\right]^{-1/2}, \quad (8)$$

$$k_v = \frac{1+i}{\delta_v}, \quad \delta_v = \sqrt{\frac{2\nu}{\omega}}, \quad \nu = \frac{\eta}{\rho_f}. \quad (9)$$

Recall that δ_v is known as the viscous penetration depth and ν is the kinematic viscosity.

The geometry of the problem (Fig. 1) suggests that φ_f and $\boldsymbol{\psi}_f$ can be represented as

$$\varphi_f = \varphi_f(x,z,t) = F(z)e^{i(kx-\omega t)}, \quad (10)$$

$$\boldsymbol{\psi}_f = \boldsymbol{e}_y \psi_f(x,z,t) = \boldsymbol{e}_y G(z) e^{i(kx-\omega t)}, \quad (11)$$

where $\boldsymbol{e}_y$ is the unit vector along the y axis and k is the wave number to be found. Substitution of Eqs. (10) and (11) into Eqs. (5) and (6) gives the following equations for $F(z)$ and $G(z)$:

$$\frac{d^2F}{dz^2} - q_f^2 F = 0, \quad \frac{d^2G}{dz^2} - q_v^2 G = 0, \quad (12)$$

where

$$q_f^2 = k^2 - k_f^2, \quad q_v^2 = k^2 - k_v^2. \quad (13)$$

Solutions to Eq. (12) are expressed in terms of the functions $\exp(\pm q_f z)$ and $\exp(\pm q_v z)$ where the first exponential function gives two independent solutions for $F(z)$ and the second function gives two independent solutions for $G(z)$. It follows that φ_f and ψ_f can be written as

$$\varphi_f = (A_1 e^{q_f z} + A_2 e^{-q_f z})e^{i(kx-\omega t)}, \quad (14)$$

$$\psi_f = (B_1 e^{q_v z} + B_2 e^{-q_v z})e^{i(kx-\omega t)}, \quad (15)$$

where $A_{1,2}$ and $B_{1,2}$ are constants to be determined by boundary conditions.

It follows from Eqs. (4), (10), and (11) that the components of $\boldsymbol{v}$ are calculated by

$$v_x = \frac{\partial \varphi_f}{\partial x} - \frac{\partial \psi_f}{\partial z}, \quad v_z = \frac{\partial \varphi_f}{\partial z} + \frac{\partial \psi_f}{\partial x}. \quad (16)$$

Substitution of Eqs. (14) and (15) into Eq. (16) yields

$$v_x = e^{i(kx-\omega t)}[ik(A_1 e^{q_f z} + A_2 e^{-q_f z}) - q_v(B_1 e^{q_v z} - B_2 e^{-q_v z})], \quad (17)$$

$$v_z = e^{i(kx-\omega t)}[q_f(A_1 e^{q_f z} - A_2 e^{-q_f z}) + ik(B_1 e^{q_v z} + B_2 e^{-q_v z})]. \quad (18)$$

2. *Waves in the solid*

The motion of the solid wall is governed by [14]

$$\rho_s \frac{\partial^2 \boldsymbol{u}}{\partial t^2} = \mu \Delta \boldsymbol{u} + (\lambda + \mu)\nabla(\nabla \cdot \boldsymbol{u}), \quad (19)$$

where $\boldsymbol{u}$ is the displacement vector, ρ_s is the wall density, and μ and λ are the Lamé coefficients. By representing $\boldsymbol{u}$ as

$$\boldsymbol{u} = \nabla \varphi_s + \nabla \times \boldsymbol{\psi}_s, \quad (20)$$

and substituting it into Eq. (19), one obtains

$$\Delta \varphi_s + k_l^2 \varphi_s = 0, \quad (21)$$

$$\Delta \boldsymbol{\psi}_s + k_t^2 \boldsymbol{\psi}_s = 0, \quad (22)$$

where k_l and k_t are the wave numbers of the longitudinal and transverse waves, respectively, given by

$$k_l = \omega\sqrt{\frac{\rho_s}{\lambda + 2\mu}}, \quad k_t = \omega\sqrt{\frac{\rho_s}{\mu}}. \quad (23)$$

Solutions for Eqs. (21) and (22) are found in the same way as those for Eqs. (5) and (6). Since the waves must decay into the depth of the solid wall (in the positive direction of z),

we obtain

$$\varphi_s = Ce^{-q_l z}e^{i(kx-\omega t)}, \tag{24}$$

$$\boldsymbol{\psi}_s = \boldsymbol{e}_y\psi_s, \quad \psi_s = De^{-q_t z}e^{i(kx-\omega t)}, \tag{25}$$

where

$$q_l^2 = k^2 - k_l^2, \quad q_t^2 = k^2 - k_t^2, \tag{26}$$

and C and D are constants to be determined by boundary conditions.

The components of $\boldsymbol{u}$ are calculated by

$$u_x = \frac{\partial\varphi_s}{\partial x} - \frac{\partial\psi_s}{\partial z}, \quad u_z = \frac{\partial\varphi_s}{\partial z} + \frac{\partial\psi_s}{\partial x}. \tag{27}$$

Substitution of Eqs. (24) and (25) into Eqs. (27) yields

$$u_x = e^{i(kx-\omega t)}(ikCe^{-q_l z} + q_t De^{-q_t z}), \tag{28}$$

$$u_z = ie^{i(kx-\omega t)}(iq_l Ce^{-q_l z} + kDe^{-q_t z}). \tag{29}$$

3. Boundary conditions for linear solutions

The boundary conditions at the reflector, which is treated as a rigid wall, are given by

$$v_x = v_z = 0 \quad \text{at } z = -h. \tag{30}$$

The boundary conditions at the fluid-solid interface where the continuity of velocities and stresses is assumed are written as

$$v_x = -i\omega u_x \quad \text{at } z = 0, \tag{31}$$

$$v_z = -i\omega u_z \quad \text{at } z = 0, \tag{32}$$

$$\sigma_{xz} = \tau_{xz} \quad \text{at } z = 0, \tag{33}$$

$$\sigma_{zz} = \tau_{zz} \quad \text{at } z = 0, \tag{34}$$

where σ_{xz} and σ_{zz} are the components of the stress tensor in the fluid and τ_{xz} and τ_{zz} are the components of the stress tensor in the solid. They are defined by [14,17]

$$\sigma_{xz} = \eta\left(\frac{\partial v_x}{\partial z} + \frac{\partial v_z}{\partial x}\right), \tag{35}$$

$$\sigma_{zz} = -p + 2\eta\frac{\partial v_z}{\partial z} + (\xi - 2\eta/3)\nabla\cdot\boldsymbol{v}, \tag{36}$$

$$\tau_{xz} = \mu\left(2\frac{\partial^2\varphi_s}{\partial x\partial z} + \frac{\partial^2\psi_s}{\partial x^2} - \frac{\partial^2\psi_s}{\partial z^2}\right), \tag{37}$$

$$\tau_{zz} = \lambda\left(\frac{\partial^2\varphi_s}{\partial x^2} + \frac{\partial^2\varphi_s}{\partial z^2}\right) + 2\mu\left(\frac{\partial^2\varphi_s}{\partial z^2} + \frac{\partial^2\psi_s}{\partial x\partial z}\right). \tag{38}$$

Substituting Eqs. (7), (17), (18), (24), and (25) into Eqs. (35)–(38), one obtains

$$\sigma_{xz} = e^{i(kx-\omega t)}\eta\big[2ikq_f(A_1e^{q_f z} - A_2e^{-q_f z}) - \big(k^2 + q_v^2\big)(B_1e^{q_v z} + B_2e^{-q_v z})\big], \tag{39}$$

$$\sigma_{zz} = e^{i(kx-\omega t)}[(2\eta k^2 - i\omega\rho_f)(A_1e^{q_f z} + A_2e^{-q_f z}) + 2i\eta kq_v(B_1e^{q_v z} - B_2e^{-q_v z})], \tag{40}$$

$$\tau_{xz} = -e^{i(kx-\omega t)}\mu\big[2ikq_l Ce^{-q_l z} + \big(k^2 + q_t^2\big)De^{-q_t z}\big], \tag{41}$$

$$\tau_{zz} = e^{i(kx-\omega t)}\mu\big[\big(k^2 + q_t^2\big)Ce^{-q_l z} - 2ikq_t De^{-q_t z}\big]. \tag{42}$$

4. Dispersion equation

Substitution of Eqs. (17), (18), (28), (29), and (39)–(42) into Eqs. (30)–(34) yields a system of six algebraic equations in the unknowns $A_{1,2}$, $B_{1,2}$, C, and D,

$$a_{n1}A_1 + a_{n2}A_2 + a_{n3}B_1 + a_{n4}B_2 + a_{n5}C + a_{n6}D = 0, \quad n = 1,2,\ldots,6. \tag{43}$$

The coefficients of Eq. (43) are given in Appendix A.

The system of Eq. (43) has nontrivial solutions only if its determinant is equal to 0. This condition gives an equation for calculating k,

$$\begin{aligned}&\big\{2\eta\omega kq_f[(\alpha_1-1)\gamma_1 - i\alpha_2\gamma_3] - \eta\omega\big(k^2+q_v^2\big)[i\alpha_3\gamma_1 + (1+\alpha_4)\gamma_3] + 2i\mu kq_l\big\}\\ &\times\{2\eta\omega kq_v[i\alpha_3\gamma_2 + (1+\alpha_4)\gamma_4] - \omega(2i\eta k^2 + \omega\rho_f)[i(1+\alpha_1)\gamma_2 + \alpha_2\gamma_4] + 2i\mu kq_t\}\\ &-\big\{2\eta\omega kq_f[i(1+\alpha_1)\gamma_2 + \alpha_2\gamma_4] - \eta\omega\big(k^2+q_v^2\big)[\alpha_3\gamma_2 - i(1+\alpha_4)\gamma_4] + \mu\big(k^2+q_t^2\big)\big\}\\ &\times\big\{\omega(2i\eta k^2 + \omega\rho_f)[(1+\alpha_1)\gamma_1 - i\alpha_2\gamma_3] + 2\eta\omega kq_v[\alpha_3\gamma_1 + i(1-\alpha_4)\gamma_3] - \mu\big(k^2+q_t^2\big)\big\} = 0.\end{aligned} \tag{44}$$

The functions appearing in Eq. (44) are calculated as follows:

$$\alpha_1 = \frac{q_f q_v + k^2}{q_f q_v - k^2}e^{-2q_f h}, \tag{45}$$

$$\alpha_2 = \frac{2ikq_v}{q_f q_v - k^2}e^{-(q_f+q_v)h}, \tag{46}$$

$$\alpha_3 = -\frac{2ikq_f}{q_f q_v - k^2}e^{-(q_f+q_v)h}, \tag{47}$$

$$\alpha_4 = \frac{q_f q_v + k^2}{q_f q_v - k^2}e^{-2q_v h}, \tag{48}$$

$$\gamma_1 = \frac{q_l q_v\beta_2 - k^2\beta_4}{k^2\beta_1\beta_4 + q_f q_v\beta_2\beta_3}, \tag{49}$$

$$\gamma_2 = \frac{k(q_v\beta_2 - q_t\beta_4)}{k^2\beta_1\beta_4 + q_f q_v\beta_2\beta_3}, \tag{50}$$

$$\gamma_3 = \frac{k(q_l\beta_1 + q_f\beta_3)}{k^2\beta_1\beta_4 + q_f q_v\beta_2\beta_3}, \tag{51}$$

$$\gamma_4 = \frac{k^2\beta_1 + q_t q_f \beta_3}{k^2\beta_1\beta_4 + q_f q_v \beta_2\beta_3}, \tag{52}$$

$$\beta_1 = \frac{q_f q_v - k^2 + (q_f q_v + k^2)e^{-2q_f h} - 2q_f q_v e^{-(q_f+q_v)h}}{q_f q_v - k^2}, \tag{53}$$

$$\beta_2 = \frac{k^2 - q_f q_v - 2k^2 e^{-(q_f+q_v)h} + (q_f q_v + k^2)e^{-2q_v h}}{q_f q_v - k^2}, \tag{54}$$

$$\beta_3 = \frac{q_f q_v - k^2 - (q_f q_v + k^2)e^{-2q_f h} + 2k^2 e^{-(q_f+q_v)h}}{q_f q_v - k^2}, \tag{55}$$

$$\beta_4 = \frac{q_f q_v - k^2 - 2q_f q_v e^{-(q_f+q_v)h} + (q_f q_v + k^2)e^{-2q_v h}}{q_f q_v - k^2}. \tag{56}$$

In the case of low viscosity, we can keep only terms of first order in δ_v. As a result, Eq. (44) reduces to

$$\left(k^2 + q_t^2\right)^2 - 4k^2 q_l q_t - \frac{\rho_f q_l k_t^4}{\rho_s \tau}\cot(h\tau) + g(k) = 0, \tag{57}$$

where $\tau = \sqrt{k_f^2 - k^2}$, $k_f = \omega/c_f$, and the function $g(k)$, which allows for viscous effects, is calculated by

$$\begin{aligned} g(k) = {} & \frac{(1+i)k^2\left(k^2+q_t^2\right)\delta_v}{2\tau^2}\left\{\frac{k_t^2\rho_f}{\rho_s}\left[\tau\ \cot(h\tau) + \frac{2q_l e^{2ih\tau}}{1-e^{2ih\tau}}\right] - i\tau\left(k^2+q_t^2\right)\right\} \\ & - \frac{(1+i)k^2 q_l \delta_v}{\tau^2}\left\{\frac{k_t^2\rho_f}{\rho_s}\left[q_t\tau\ \cot(h\tau) + \frac{2k^2 e^{2ih\tau}}{1-e^{2ih\tau}}\right] - 2ik^2\tau q_t\right\} \\ & + \frac{(1-i)\delta_v}{2\tau^2}\left\{\frac{ik_t^2\rho_f}{\rho_s}[k^2\cot(h\tau) - \tau q_t] + k^2\left(k^2+q_t^2\right)\right\}\left[\frac{q_l k_t^2\rho_f}{\rho_s}\cot(h\tau) + \tau\left(k^2+q_t^2\right)\right] \\ & - \frac{(1-i)k^2\delta_v}{2\tau^2}\left\{\frac{ik_t^2\rho_f}{\rho_s}[q_l\cot(h\tau) - \tau] + 2k^2 q_l\right\}\left[\frac{k_t^2\rho_f}{\rho_s}\cot(h\tau) + 2\tau q_t\right]. \end{aligned} \tag{58}$$

The wave number of a leaky surface wave should be a complex number, which provides the formation of a wave departing from the boundary into the fluid [14]. For an inviscid fluid layer, theoretically, such solutions exist if the fluid layer is of infinite thickness. The dispersion equation for this case is given by Viktorov [14],

$$\left(k^2 + q_t^2\right)^2 - 4k^2 q_l q_t + \frac{i\rho_f q_l k_t^4}{\rho_s \tau} = 0. \tag{59}$$

Note that for $h \to \infty$, $\cot(h\tau) \to -i$, and at $\eta = 0$, Eq. (57) turns into Eq. (59).

Qi [15] considered the case of a finite viscous fluid layer with a free surface. He derived a dispersion equation up to viscous corrections of first order,

$$\begin{aligned} & \left(k^2+q_t^2\right)^2 - 4k^2 q_l q_t + \frac{\rho_f k_t^4 q_l}{\rho_s\tau}\tan(h\tau) - \frac{(1+i)\sqrt{\omega\nu}}{\sqrt{2}c_t\tau} \\ & \times \tan(h\tau)\left[\frac{k^2}{k_t}\left[\left(k^2+q_t^2\right)^2 - 4k^2 q_l q_t\right]\right. \\ & + \frac{2\rho_f}{\rho_s}k^2 k_t\left(k^2+q_t^2-2q_l q_t\right) \\ & \left. + \left(\frac{\rho_f}{\rho_s}\right)^2 k_t^3(k^2 - q_l q_t)\right] + \frac{(1+i)\rho_f k_t^3 q_t\sqrt{\omega\nu}}{\sqrt{2}\rho_s c_t} = 0. \end{aligned} \tag{60}$$

It is instructive to compare the predictions of Eq. (57) with those of Eqs. (59) and (60). The comparison is presented in Figs. 2 and 3. The following parameters were used: $\rho_f = 1000\,\mathrm{kg/m^3}$, $c_f = 1500\,\mathrm{m/s}$, $\eta = 0.001$, $\xi = 0.003\,\mathrm{Pa\,s}$, $\rho_s = 4640\,\mathrm{kg/m^3}$, $\lambda = 68$, $\mu = 68\,\mathrm{GPa}$, and $f = \omega/2\pi = 36\,\mathrm{MHz}$. These parameters correspond to water (fluid layer) and lithium niobate (solid wall). Figure 2 shows the speed of the acoustic wave in the microfluidic channel $c = \omega/\mathrm{Re}[k]$ as a function of the channel height h, and Fig. 3 shows the attenuation coefficient $\alpha = \mathrm{Im}[k]$ as a function of h. The solid lines depict the results calculated by Eq. (57), the long-dashed lines are provided by Eq. (59), and the short-dashed lines correspond to Eq. (60). The breaks in the

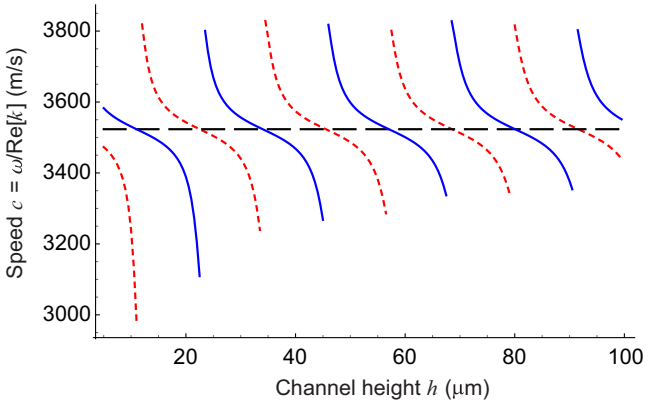

FIG. 2. Speed of the acoustic wave in the microfluidic channel versus channel height for three cases: a fluid layer with a reflector (solid line), a fluid layer with a free boundary (short-dashed line), and an infinite inviscid fluid layer (long-dashed line).

solid and short-dashed curves are caused by singularities in $\cot(h\tau)$ and $\tan(h\tau)$. As one can see from Figs. 2 and 3, the case of a fluid layer with a reflector differs greatly from the other two cases.

$$A_1 = \omega(i\gamma_1 C + \gamma_2 D), \tag{61}$$

$$A_2 = \omega[(i\alpha_1\gamma_1 + \alpha_2\gamma_3)C + (\alpha_1\gamma_2 - i\alpha_2\gamma_4)D], \tag{62}$$

$$B_1 = \omega(\gamma_3 C - i\gamma_4 D), \tag{63}$$

$$B_2 = \omega[(i\alpha_3\gamma_1 + \alpha_4\gamma_3)C + (\alpha_3\gamma_2 - i\alpha_4\gamma_4)D], \tag{64}$$

$$D = \frac{\eta\omega\{(k^2+q_v^2)[i\alpha_3\gamma_1 + (1+\alpha_4)\gamma_3] + 2kq_f[(1-\alpha_1)\gamma_1 + i\alpha_2\gamma_3]\} - 2i\mu k q_l}{\eta\omega\{2kq_f[i(1+\alpha_1)\gamma_2 + \alpha_2\gamma_4] - (k^2+q_v^2)[\alpha_3\gamma_2 - i(1+\alpha_4)\gamma_4]\} + \mu(k^2+q_t^2)} C. \tag{65}$$

6. Standing wave

Let a second leaky wave propagate in the negative direction of the x axis. The potential functions that describe this process can be represented as

$$\hat{\varphi}_f = (\hat{A}_1 e^{q_f z} + \hat{A}_2 e^{-q_f z}) e^{i(-kx-\omega t)},$$

$$\hat{\psi}_f = (\hat{B}_1 e^{q_v z} + \hat{B}_2 e^{-q_v z}) e^{i(-kx-\omega t)}, \tag{66}$$

$$\hat{\varphi}_s = \hat{C} e^{-q_l z} e^{i(-kx-\omega t)}, \quad \hat{\psi}_s = \hat{D} e^{-q_t z} e^{i(-kx-\omega t)}. \tag{67}$$

To get a combined standing wave, we set $\hat{C} = C$. The other constants are found from Eqs. (61)–(65) by replacing k with $-k$: $\hat{D} = -D$, $\hat{A}_1 = A_1$, $\hat{A}_2 = A_2$, $\hat{B}_1 = -B_1$, and $\hat{B}_2 = -B_2$. As a result, the components of the total displacement in the solid wall are given by

$$u_x = 2ie^{-i\omega t}(ikCe^{-q_l z} + q_t De^{-q_t z})\sin(kx), \tag{68}$$

$$u_z = 2ie^{-i\omega t}(iq_l Ce^{-q_l z} + kDe^{-q_t z})\cos(kx), \tag{69}$$

and those of the total fluid velocity are written as

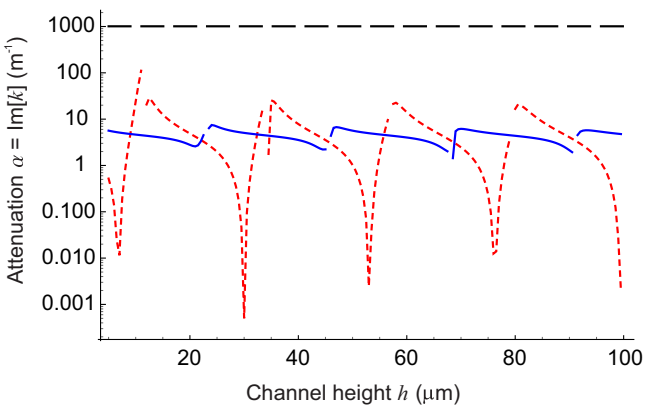

FIG. 3. Attenuation of the acoustic wave in the microfluidic channel versus channel height for three cases: a fluid layer with a reflector (solid line), a fluid layer with a free boundary (short-dashed line), and an infinite inviscid fluid layer (long-dashed line).

5. Calculation of constants

The system of Eq. (43) also allows one to express $A_{1,2}$, $B_{1,2}$, C, and D in terms of one of these quantities. Choosing C as such a quantity, one obtains

$$v_x = 2ie^{-i\omega t}[ik(A_1 e^{q_f z} + A_2 e^{-q_f z}) - q_v(B_1 e^{q_v z} - B_2 e^{-q_v z})]\sin(kx), \tag{70}$$

$$v_z = 2e^{-i\omega t}[q_f(A_1 e^{q_f z} - A_2 e^{-q_f z}) + ik(B_1 e^{q_v z} + B_2 e^{-q_v z})]\cos(kx). \tag{71}$$

It is seen that we really get a standing wave along the x axis. Although k is a complex number, the attenuation is weak and therefore practically does not manifest itself within the dimensions of microfluidic devices.

To facilitate calculations that follow, Eqs. (70) and (71) are represented by

$$v_x = 2ie^{-i\omega t}[iks_1(z) - q_v s_2(z)]\sin(kx), \tag{72}$$

$$v_z = 2e^{-i\omega t}[q_f s_3(z) + iks_4(z)]\cos(kx), \tag{73}$$

where

$$s_1(z) = A_1 e^{q_f z} + A_2 e^{-q_f z}, \tag{74}$$

$$s_2(z) = B_1 e^{q_v z} - B_2 e^{-q_v z}, \tag{75}$$

$$s_3(z) = A_1 e^{q_f z} - A_2 e^{-q_f z}, \tag{76}$$

$$s_4(z) = B_1 e^{q_v z} + B_2 e^{-q_v z}. \tag{77}$$

Note that the functions $s_n(z)$ obey the following identities:

$$s_1' = q_f s_3, \quad s_2' = q_v s_4, \quad s_3' = q_f s_1, \quad s_4' = q_v s_2, \tag{78}$$

where the prime denotes the derivative with respect to z. These identities will be used in the calculation of acoustic streaming.

C. Acoustic streaming

1. Solutions of the equations of acoustic streaming

The equations of acoustic streaming are given by [18]

$$\nabla \cdot \boldsymbol{V} = 0, \tag{79}$$

$$\nu\Delta\boldsymbol{V} - \frac{1}{\rho_f}\nabla P = \langle(\boldsymbol{v}\cdot\nabla)\boldsymbol{v}\rangle, \tag{80}$$

where $\boldsymbol{V}$ and P are the Eulerian velocity and the pressure of the acoustic streaming and $\langle\rangle$ means time averaging. To satisfy Eq. (79), we set

$$\boldsymbol{V} = \nabla \times \boldsymbol{\Psi}. \tag{81}$$

Substituting Eq. (81) into Eq. (80) and applying the curl operator, one obtains

$$\Delta^2 \boldsymbol{\Psi} = -\frac{1}{\nu}\nabla \times \boldsymbol{W}, \tag{82}$$

where

$$\boldsymbol{W} = \langle (\boldsymbol{v}\cdot\nabla)\boldsymbol{v}\rangle. \tag{83}$$

The geometry of the problem allows one to write

$$\boldsymbol{\Psi} = \Psi(x,z)\boldsymbol{e}_y, \tag{84}$$

so the velocity components are given by

$$V_x = -\frac{\partial \Psi}{\partial z}, \quad V_z = \frac{\partial \Psi}{\partial x}. \tag{85}$$

Substituting Eq. (84) into Eq. (82) and considering that

$$\boldsymbol{W} = W_x(x,z)\boldsymbol{e}_x + W_z(x,z)\boldsymbol{e}_z, \tag{86}$$

one obtains

$$\Delta^2 \Psi = \frac{1}{\nu}\left(\frac{\partial W_z}{\partial x} - \frac{\partial W_x}{\partial z}\right), \tag{87}$$

where, as follows from Eq. (83),

$$\begin{aligned} W_x &= \frac{1}{2}\mathrm{Re}\left\{v_x^*\frac{\partial v_x}{\partial x} + v_z^*\frac{\partial v_x}{\partial z}\right\}, \\ W_z &= \frac{1}{2}\mathrm{Re}\left\{v_x^*\frac{\partial v_z}{\partial x} + v_z^*\frac{\partial v_z}{\partial z}\right\}, \end{aligned} \tag{88}$$

with the asterisks denoting the complex conjugates.

Substituting Eqs. (72) and (73) into Eq. (88) and then into Eq. (87) after cumbersome but straightforward rearrangements, one obtains

$$\begin{aligned} \Delta^2\Psi = \frac{1}{\nu}\mathrm{Re}\big\{ & k_v^2 \sin(2k_R x)\big[i\left(|k|^2 + k_f^2\right)s_1 s_4^* - iq_f q_v^* s_2^* s_3 \\ & + 2kq_v^* s_2^* s_4\big] + k_v^2 \sin(2ik_I x)\big[i\left(|k|^2 - k_f^2\right)s_1 s_4^* \\ & + iq_f q_v^* s_2^* s_3 - 2kq_v^* s_2^* s_4\big]\big\}, \end{aligned} \tag{89}$$

where $k_R = \mathrm{Re}\{k\}$ and $k_I = \mathrm{Im}\{k\}$. Equation (89) suggests that Ψ should be sought in the following form:

$$\Psi = \frac{1}{\nu}\mathrm{Re}\big\{k_v^2[F_1(z)\sin(2k_R x) + F_2(z)\sin(2ik_I x)]\big\}. \tag{90}$$

Substitution of Eq. (90) into Eq. (89) yields equations for F_1 and F_2,

$$\begin{aligned} & \frac{d^4F_1}{dz^4} - 8k_R^2\frac{d^2F_1}{dz^2} + 16k_R^4 F_1 \\ & \quad = i\left(|k|^2 + k_f^2\right)s_1 s_4^* - iq_f q_v^* s_2^* s_3 + 2kq_v^* s_2^* s_4, \end{aligned} \tag{91}$$

$$\begin{aligned} & \frac{d^4F_2}{dz^4} + 8k_I^2\frac{d^2F_2}{dz^2} + 16k_I^4 F_2 \\ & \quad = i\left(|k|^2 - k_f^2\right)s_1 s_4^* + iq_f q_v^* s_2^* s_3 - 2kq_v^* s_2^* s_4. \end{aligned} \tag{92}$$

Analysis of Eqs. (91) and (92) reveals that particular solutions for these equations can be written as

$$f_n(z) = f_{n1}s_1 s_4^* + f_{n2}s_2^* s_3 + f_{n3}s_2^* s_4 + f_{n4}s_2 s_4^*, \tag{93}$$

where $n = 1,2$ and f_{nm}'s are constants. The constants are calculated by substituting Eq. (93) into Eqs. (91) and (92) and using Eqs. (78). The resulting expressions are provided in Appendix B.

The general solution of a nonhomogeneous differential equation is known to be a sum of its particular solution and solutions for the homogeneous equation corresponding to the equation being considered, i.e., solutions for the same equation with a zero right side. According to this rule, the general solutions of Eqs. (91) and (92) are given by

$$F_1(z) = f_1(z) + (c_{11} + c_{12}z)e^{2k_R z} + (c_{13} + c_{14}z)e^{-2k_R z}, \tag{94}$$

$$F_2(z) = f_2(z) + (c_{21} + c_{22}z)e^{2ik_I z} + (c_{23} + c_{24}z)e^{-2ik_I z}, \tag{95}$$

where c_{nm}'s are constants to be determined by boundary conditions.

By using Eq. (85), one obtains the velocity components of the streaming,

$$V_x = -\frac{1}{\nu}\mathrm{Re}\big\{k_v^2[F_1'(z)\sin(2k_R x) + F_2'(z)\sin(2ik_I x)]\big\}, \tag{96}$$

$$V_z = \frac{2}{\nu}\mathrm{Re}\big\{k_v^2[k_R F_1(z)\cos(2k_R x) + ik_I F_2(z)\cos(2ik_I x)]\big\}. \tag{97}$$

Expressions for the derivatives F_n' are given in Appendix C.

The constants c_{nm} in Eqs. (94) and (95) are calculated by the boundary conditions for V_x and V_z at the reflector and at the solid wall. However, the boundary conditions should be applied to the Lagrangian streaming velocity, which is the sum of the Eulerian streaming velocity and the Stokes drift velocity. Therefore, the Stokes drift velocity is calculated in the next subsection.

2. *Stokes drift velocity*

The Stokes drift velocity is calculated by [19]

$$\boldsymbol{V}_S = \left\langle \int \boldsymbol{v}\, dt\cdot\nabla\boldsymbol{v}\right\rangle = \frac{1}{\omega}\langle (i\boldsymbol{v}\cdot\nabla)\boldsymbol{v}\rangle. \tag{98}$$

Substitution of Eqs. (72) and (73) into Eq. (98) yields

$$V_{Sx} = \frac{1}{\omega}\mathrm{Re}\{G_1(z)[\sin(2ik_I x) - \sin(2k_R x)]\}, \tag{99}$$

$$V_{Sz} = \frac{1}{\omega}\mathrm{Re}\{G_2(z)\cos(2k_R x) + G_3(z)\cos(2ik_I x)\}, \tag{100}$$

where

$$G_1(z) = ik|ks_1 + iq_v s_2|^2 + (iq_f s_3 - ks_4)\left(kq_f s_3 + iq_v^2 s_4\right)^*, \tag{101}$$

$$G_2(z) = \left[\left(q_f^2 + |k|^2\right)s_1 + 2ik_R q_v s_2\right](iq_f s_3 - ks_4)^*, \tag{102}$$

$$G_3(z) = \left[\left(q_f^2 - |k|^2\right)s_1 - 2k_I q_v s_2\right](iq_f s_3 - ks_4)^*. \tag{103}$$

3. Boundary conditions for acoustic streaming

The boundary conditions for the acoustic streaming are given by [16,20]

$$\boldsymbol{V} + \boldsymbol{V}_S = 0 \quad \text{at } z = 0 \quad \text{and} \quad z = -h. \tag{104}$$

Substitution of Eqs. (96), (97), (99), and (100) into Eq. (104) yields

$$\frac{k_v^2}{\nu} F_1'(z) + \frac{1}{\omega} G_1(z) = 0 \quad \text{at } z = 0 \quad \text{and} \quad z = -h, \tag{105}$$

$$\frac{k_v^2}{\nu} F_2'(z) - \frac{1}{\omega} G_1(z) = 0 \quad \text{at } z = 0 \quad \text{and} \quad z = -h, \tag{106}$$

$$\frac{2}{\nu} k_v^2 k_R F_1(z) + \frac{1}{\omega} G_2(z) = 0 \quad \text{at } z = 0 \quad \text{and} \quad z = -h, \tag{107}$$

$$\frac{2i}{\nu} k_v^2 k_I F_2(z) + \frac{1}{\omega} G_3(z) = 0 \quad \text{at } z = 0 \quad \text{and} \quad z = -h. \tag{108}$$

These equations allows one to calculate the constants c_{nm} appearing in Eqs. (94) and (95). Equations (105) and (107) give a system of equations in c_{1m},

$$\begin{pmatrix} 2k_R & 1 & -2k_R & 1 \\ 1 & 0 & 1 & 0 \\ 2k_R e^{-2k_R h} & (1-2k_R h)e^{-2k_R h} & -2k_R e^{2k_R h} & (1+2k_R h)e^{2k_R h} \\ e^{-2k_R h} & -he^{-2k_R h} & e^{2k_R h} & -he^{2k_R h} \end{pmatrix} \times \begin{pmatrix} c_{11} \\ c_{12} \\ c_{13} \\ c_{14} \end{pmatrix} = \begin{pmatrix} -\frac{\nu G_1(0)}{\omega k_v^2} - f_1'(0) \\ -\frac{\nu G_2(0)}{2\omega k_v^2 k_R} - f_1(0) \\ -\frac{\nu G_1(-h)}{\omega k_v^2} - f_1'(-h) \\ -\frac{\nu G_2(-h)}{2\omega k_v^2 k_R} - f_1(-h) \end{pmatrix}. \tag{109}$$

The unknowns c_{1m} are calculated by

$$c_{1m} = \frac{D_{1m}}{D_1}, \tag{110}$$

where D_1 is the determinant of the coefficient matrix of Eq. (109) and D_{1m} is the determinant of the coefficient matrix in which the mth column is replaced with the column of the free terms.

A system of equations in c_{2m} is given by Eqs. (106) and (108),

$$\begin{pmatrix} 2ik_I & 1 & -2ik_I & 1 \\ 1 & 0 & 1 & 0 \\ 2ik_I e^{-2ik_I h} & (1-2ik_I h)e^{-2ik_I h} & -2ik_I e^{2ik_I h} & (1+2ik_I h)e^{2ik_I h} \\ e^{-2ik_I h} & -he^{-2ik_I h} & e^{2ik_I h} & -he^{2ik_I h} \end{pmatrix} \times \begin{pmatrix} c_{21} \\ c_{22} \\ c_{23} \\ c_{24} \end{pmatrix} = \begin{pmatrix} \frac{\nu G_1(0)}{\omega k_v^2} - f_2'(0) \\ \frac{i\nu G_3(0)}{2\omega k_v^2 k_I} - f_2(0) \\ \frac{\nu G_1(-h)}{\omega k_v^2} - f_2'(-h) \\ \frac{i\nu G_3(-h)}{2\omega k_v^2 k_I} - f_2(-h) \end{pmatrix}. \tag{111}$$

The unknowns c_{2m} are calculated by

$$c_{2m} = \frac{D_{2m}}{D_2}, \tag{112}$$

where the meaning of D_2 and D_{2m} is analogous to that of D_1 and D_{1m}.

The calculation of the constants c_{nm} completes the calculation of the acoustic streaming, so the aim of our derivation is achieved.

III. NUMERICAL EXAMPLES

In the present section, the analytical theory developed above is applied to reveal the structure of the acoustic streaming by analyzing particular numerical examples. The following parameters were used: $\rho_f = 1000\,\mathrm{kg/m^3}$, $c_f = 1500\,\mathrm{m/s}$, $\eta = 0.001$, $\xi = 0.003\,\mathrm{Pa\,s}$, $\rho_s = 4640\,\mathrm{kg/m^3}$, $\lambda = 68$, $\mu = 68\,\mathrm{GPa}$, $f = \omega/2\pi = 36\,\mathrm{MHz}$, and $h = 50\,\mu\mathrm{m}$. These values are typical of microfluidic experiments [21]. For these parameters, the viscous penetration depth is $\delta_v = 94\,\mathrm{nm}$, the longitudinal wave speed is $c_l = 6630.65\,\mathrm{m/s}$, the transverse wave speed is $c_t = 3828.21\,\mathrm{m/s}$, and the dispersion equation Eq. (57) gives the wave number of the leaky surface wave $k = 62859 + 5.64i\,\mathrm{m^{-1}}$, which corresponds to the wave speed $c = \omega/\mathrm{Re}[k] = 3598.45\,\mathrm{m/s}$, the wavelength $\lambda_{sw} = 99.96\,\mu\mathrm{m}$, and the attenuation coefficient $\alpha = \mathrm{Im}[k] = 5.64\,\mathrm{m^{-1}}$. The low attenuation appears to be a result of reflections from the rigid upper boundary. The radiation angle of the leaky surface wave, as follows from Snell's law $\cos\,\theta = c_f/c$, is $\theta \approx 65^\circ$.

The x dependence of the linear solutions, given by Eqs. (72) and (73), is absolutely clear: Both components of the fluid velocity behave as a sinusoidal standing wave along the x axis. Hence, there is little point in graphically representing their x dependences. The behavior of the linear solutions along the z axis is less explicit. Therefore, it is illustrated in Fig. 4 where the amplitudes of v_x and v_z are depicted as functions of z. Note that the label 1.0 on the vertical axis in Fig. 4 corresponds to the position of the reflector. The

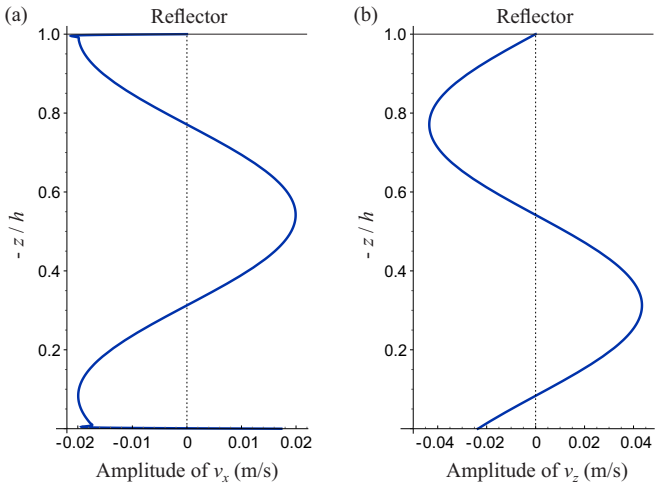

FIG. 4. The amplitudes of the components of the linear fluid velocity as functions of z.

value of C was set equal to 1.25×10^{-15} m^2. At this value, the magnitude of the vertical displacement of the solid-fluid interface is about 0.1 nm as in the numerical simulations performed in Ref. [16]. This choice is somewhat arbitrary because the vertical displacements of the solid boundary are difficult to measure experimentally [16]. Figure 4 shows that v_x undergoes strong jumps near the boundaries in order to achieve the matching with the boundary velocities. The enlarged views of the boundary regions are shown in Fig. 5. The abrupt change in v_x in these regions is caused by the fact that the bulk fluid motion along the x axis is in effect nonviscous. Only within very narrow boundary layers ($\delta_v \approx 0.002h$) do viscous effects begin to act.

Figure 6 shows the contour plot of the Eulerian stream function $\Psi(x,z)$ given by Eq. (90). The streamline pattern corresponding to Fig. 6 is presented in Fig. 7. As one can see, two vortex systems are established along the boundaries of the channel. The vortices are located with a step of $\lambda_{sw}/4$ along the x axis.

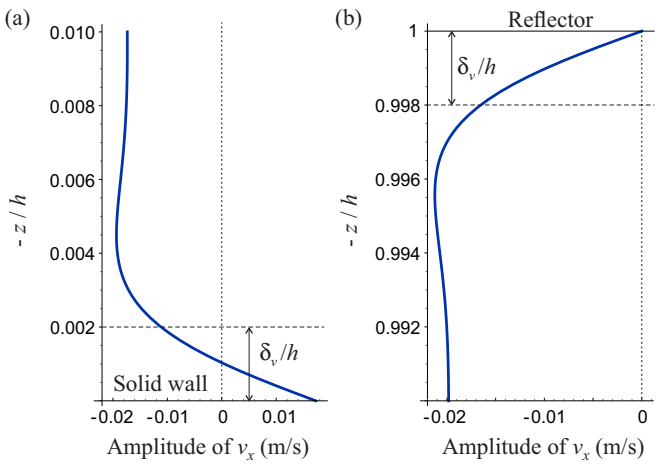

FIG. 5. Behavior of the linear fluid velocity within the boundary layer (a) at the solid wall and (b) at the reflector.

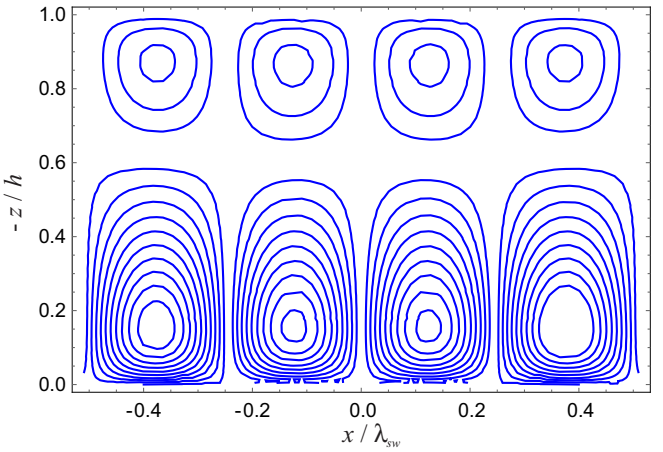

FIG. 6. Contour plot of the Eulerian stream function $\Psi(x,z)$ given by Eq. (90).

Figure 8 illustrates the dependence of the streaming pattern on the channel height h. Although h changes in a rather wide range from 10 to 200 μm, qualitatively, the streaming behavior remains the same. Two rows of vortices persist along the boundaries of the channel. However, their form changes with changing h. At higher h, the vortices become more pressed against the boundaries. The absence of lines in the middle part of the plots in the left panel of Fig. 8 means that the value of $\Psi(x,z)$ is very small there. The right panel in Fig. 8 shows that the streamlined patterns become more sophisticated with increasing h.

IV. CONCLUSION

A theory has been developed for the modeling of acoustic streaming in a microfluidic channel confined between an elastic solid wall and a rigid reflector. The theory assumes that the acoustic streaming is generated by a standing wave that is created by two counterpropagating leaky surface waves induced in the solid wall as is the case in microfluidic devices. A dispersion equation was derived that allows one to calculate the speed of leaky surface waves in the case under consideration. Analytical solutions were obtained for

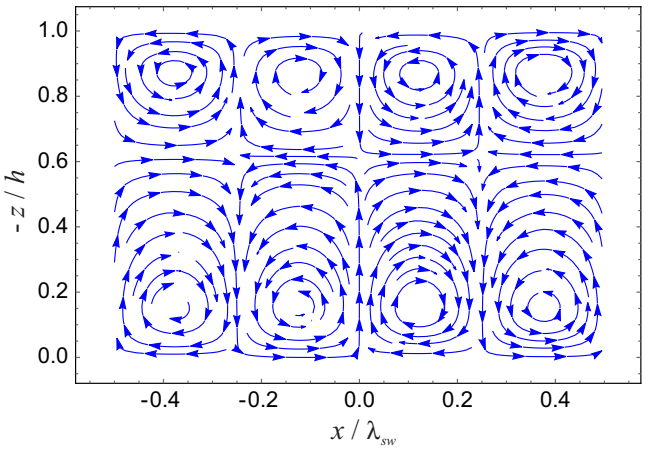

FIG. 7. Streamlines in the case shown in Fig. 6. Two systems of vortices are established along the boundaries of the channel.

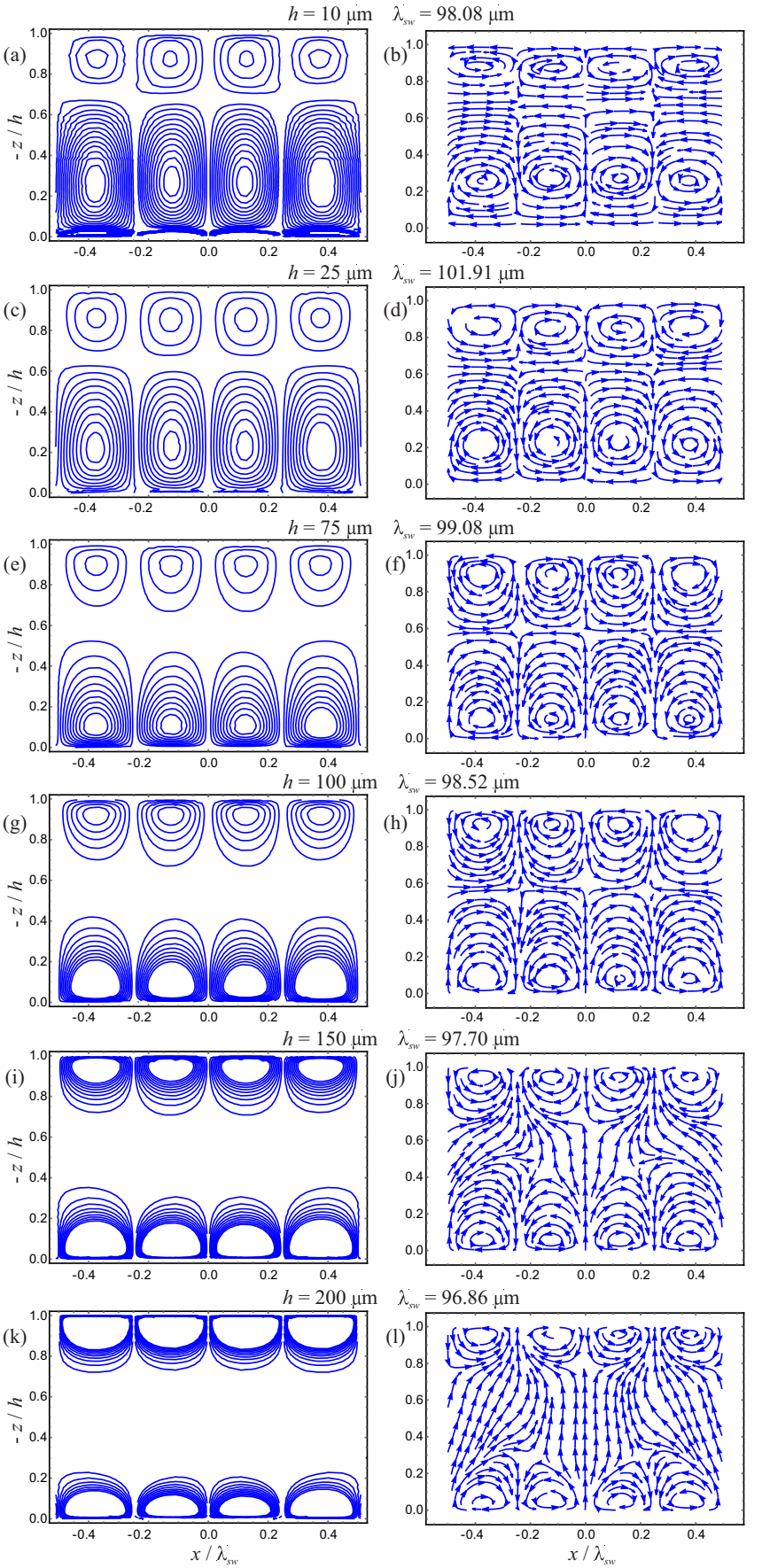

FIG. 8. Streaming behavior at different values of the channel height h. Left panel: Contour plots of the Eulerian stream function $\Psi(x,z)$. Right panel: Streamline patterns.

all the processes involved: wave propagation in the solid, linear acoustic waves in the fluid, and the time-averaged fluid flow. Particular numerical examples were considered to reveal the structure of the acoustic streaming. It was found that two systems of vortices were established along the boundaries of the microchannel.

ACKNOWLEDGMENT

This research has received funding from the European Research Council under the European Union's Seventh Framework Programme (FP7/2007-2013)/ERC Grant Agreement No. 614655 "Bubbleboost."

APPENDIX A: COEFFICIENT MATRIX OF EQ. (43)

$$a_{nm} = \begin{pmatrix} ike^{-q_f h} & ike^{q_f h} & -q_v e^{-q_v h} & q_v e^{q_v h} & 0 & 0 \\ q_f e^{-q_f h} & -q_f e^{q_f h} & ike^{-q_v h} & ike^{q_v h} & 0 & 0 \\ ik & ik & -q_v & q_v & -\omega k & i\omega q_t \\ q_f & -q_f & ik & ik & -i\omega q_l & -\omega k \\ 2i\eta k q_f & -2i\eta k q_f & -\eta\left(k^2+q_v^2\right) & -\eta\left(k^2+q_v^2\right) & 2i\mu k q_l & \mu\left(k^2+q_t^2\right) \\ 2\eta k^2 - i\omega\rho_f & 2\eta k^2 - i\omega\rho_f & 2i\eta k q_v & -2i\eta k q_v & -\mu\left(k^2+q_t^2\right) & 2i\mu k q_t \end{pmatrix}.$$

APPENDIX B: EXPRESSIONS FOR f_{nm}

The constants f_{1m} and f_{2m} ($m = 1$–4), which appear in Eq. (91), are calculated by

$$f_{11} = \frac{i\left(|k|^2+k_f^2\right)m_1 + iq_f q_v^* m_2}{m_1^2 - m_2^2}, \quad f_{12} = -\frac{iq_f q_v^* m_1 + i\left(|k|^2+k_f^2\right)m_2}{m_1^2 - m_2^2}, \tag{B1}$$

$$f_{13} = \frac{2kq_v^* m_3}{m_3^2 - m_4^2}, \quad f_{14} = -\frac{2kq_v^* m_4}{m_3^2 - m_4^2}, \tag{B2}$$

$$f_{21} = \frac{i\left(|k|^2-k_f^2\right)n_1 - iq_f q_v^* n_2}{n_1^2 - n_2^2}, \quad f_{22} = \frac{iq_f q_v^* n_1 - i\left(|k|^2-k_f^2\right)n_2}{n_1^2 - n_2^2}, \tag{B3}$$

$$f_{23} = -\frac{2kq_v^* n_3}{n_3^2 - n_4^2}, \quad f_{24} = \frac{2kq_v^* n_4}{n_3^2 - n_4^2}, \tag{B4}$$

where

$$m_1 = q_f^4 + q_v^{4*} + 6q_f^2 q_v^{2*} + 8k_R^2\left(2k_R^2 - q_f^2 - q_v^{2*}\right), \quad m_2 = 4q_f q_v^*\left(q_f^2 + q_v^{2*} - 4k_R^2\right), \tag{B5}$$

$$m_3 = q_v^4 + q_v^{4*} + 6q_v^2 q_v^{2*} + 8k_R^2\left(2k_R^2 - q_v^2 - q_v^{2*}\right), \quad m_4 = 4q_v q_v^*\left(q_v^2 + q_v^{2*} - 4k_R^2\right), \tag{B6}$$

$$n_1 = q_f^4 + q_v^{4*} + 6q_f^2 q_v^{2*} + 8k_I^2\left(2k_I^2 + q_f^2 + q_v^{2*}\right), \quad n_2 = 4q_f q_v^*\left(q_f^2 + q_v^{2*} + 4k_I^2\right), \tag{B7}$$

$$n_3 = q_v^4 + q_v^{4*} + 6q_v^2 q_v^{2*} + 8k_I^2\left(2k_I^2 + q_v^2 + q_v^{2*}\right), \quad n_4 = 4q_v q_v^*\left(q_v^2 + q_v^{2*} + 4k_I^2\right). \tag{B8}$$

APPENDIX C: DERIVATIVES OF F_n

$$F_n'(z) = f_n'(z) + [2k_R c_{11} + c_{12}(1+2k_R z)]e^{2k_R z} - [2k_R c_{13} - c_{14}(1-2k_R z)]e^{-2k_R z}, \tag{C1}$$

$$F_2'(z) = f_2'(z) + [2ik_I c_{21} + c_{22}(1+2ik_I z)]e^{2ik_I z} - [2ik_I c_{23} - c_{24}(1-2ik_I z)]e^{-2ik_I z}, \tag{C2}$$

$$f_n'(z) = (q_v^* f_{n1} + q_f f_{n2})s_1 s_2^* + (q_v f_{n3} + q_v^* f_{n4})s_2 s_2^* + (q_f f_{n1} + q_v^* f_{n2})s_3 s_4^* + (q_v^* f_{n3} + q_v f_{n4})s_4 s_4^*. \tag{C3}$$

[1] J. Friend and L. Yeo, Rev. Mod. Phys. **83**, 647 (2011).
[2] C. Wang, S. V. Jalikop, and S. Hilgenfeldt, Appl. Phys. Lett. **99**, 034101 (2011).
[3] J. Lei, P. Glynne-Jones, and M. Hill, Lab Chip **13**, 2133 (2013).
[4] J. Lei, M. Hill, and P. Glynne-Jones, Lab Chip **14**, 532 (2014).
[5] N. Nama, R. Barnkob, Z. Mao, C. J. Kähler, F. Costanzo, and T. J. Huang, Lab Chip **15**, 2700 (2015).
[6] A. Lamprecht, S. Lakämper, T. Baasch, I. A. T. Schaap, and J. Dual, Lab Chip **16**, 2682 (2016).
[7] Lord Rayleigh, Philos. Trans. R. Soc. London **175**, 1 (1884).
[8] P. J. Westervelt, J. Acoust. Soc. Am. **25**, 60 (1953).

[9] W. L. Nyborg, in *Physical Acoustics*, edited by W. P. Mason (Academic, New York, 1965), Vol. 2B, Chap. 11, pp. 290–295.
[10] W. L. Nyborg, in *Nonlinear Acoustics*, edited by M. F. Hamilton and D. T. Blackstock (Academic, San Diego, 1998), Chap. 7, Sec. 3.3.
[11] M. F. Hamilton, Y. A. Ilinskii, and E. A. Zabolotskaya, J. Acoust. Soc. Am. **113**, 153 (2003).
[12] A. A. Doinikov, P. Thibault, and P. Marmottant, J. Acoust. Soc. Am. **141**, 1282 (2017).
[13] S. B. Q. Tran, P. Marmottant, and P. Thibault, Appl. Phys. Lett. **101**, 114103 (2012).
[14] I. A. Viktorov, *Rayleigh and Lamb Waves: Physical Theory and Applications* (Plenum, New York, 1967).
[15] Q. Qi, J. Acoust. Soc. Am. **95**, 3222 (1994).
[16] J. Vanneste and O. Bühler, Proc. R. Soc. A **467**, 1779 (2011).
[17] L. D. Landau and E. M. Lifshitz, *Fluid Mechanics* (Pergamon, Oxford, 1987).
[18] S. J. Lighthill, J. Sound Vib. **61**, 391 (1978).
[19] M. S. Longuet-Higgins, Proc. R. Soc. London, Ser. A **454**, 725 (1998).
[20] C. E. Bradley, J. Acoust. Soc. Am. **100**, 1399 (1996).
[21] I. Bernard, A. A. Doinikov, P. Marmottant, D. Rabaud, C. Poulain, and P. Thibault, Lab Chip (2017).